THE RESULTS OF THE SPECIALISTS' AND SCIENTISTS' RESEARCHES

Original article
https://doi.org/10.15828/2075-8545-2022-14-6-455-465

Fabrication of W nanodot and Nitrogen Co-decorated Carbon Skeleton for Hydrogen Evolution Reaction

Yange Wang[1], Yechen Wang[1], Jing Bai[1, 2] *, Sibin Duan[1] *, Rongming Wang[1] *, Woon-Ming Lau[1, 2] *

[1] Beijing Advanced Innovation Center for Materials Genome Engineering, Beijing Key Laboratory for Magneto-Photoelectrical Composite and Interface Science, Center for Green Innovation, University of Science and Technology Beijing, Beijing, 100083, China

[2] Shunde Graduate School of University of Science and Technology Beijing, Foshan 528000, China

* Corresponding authors: e-mail: xingqingcaoyuan@163.com (Jing Bai), sibinduan@ustb.edu.cn (Sibin Duan), rmwang@ustb.edu.cn (Rongming Wang), leolau@ustb.edu.cn (Woon-Ming Lau)

ABSTRACT: Metal dots-nitrogen-carbon catalysts have become a hot topic in recent years because of special coordination environment. Herein, for the study the W nanodots and nitrogen co-decorated carbon skeleton (W@NC) was prepared for hydrogen evolution reaction (HER). In particular, NaCl templates not only restrict the growth of nanodots, but also improve the purity of phase. By optimizing the feeding ratio of ammonium metatungstate, W nanodots (the size is about 1.2 ± 0.6 nm) dispersed well on N-doped C skeleton, and this special structure could effectively promote electron transfer and ion diffusion during HER process. As a result, the optimized W@NC hybrids exhibited excellent HER performance in alkaline media with a rather low over-potential (228 mV at 10 mA cm^{-2}) and outstanding durability over 10 h.

KEY WORDS: W nanodots; N-doped carbon skeleton; NaCl template; Freeze-drying; Hydrogen evolution reaction.

ACKNOWLEDGEMENTS: This research was funded by the National Natural Science Foundation of China (Nos. 51901012, 51971025 and 12034002), Beijing Natural Science Foundation (2212034), the post-doctor Research Foundation of Shunde Graduate School of University of Science and Technology Beijing (2020BH007), Foshan Talents Special Foundation (BKBS202003), Foshan Science and Technology Innovation Project (2018IT100363), the Fundamental Research Funds for the Central Universities (FRF-BD-20-13A and FRF-TP-20-011A1) and 111 Project (B170003).

FOR CITATION: Yange Wang, Yechen Wang, Jing Bai, Sibin Duan, Rongming Wang, Woon-Ming Lau. Fabrication of W nanodot and Nitrogen Co-decorated Carbon Skeleton for Hydrogen Evolution Reaction. *Nanotechnologies in Construction.* 2022; 14(6): 455–465. https://doi.org/10.15828/2075-8545-2022-14-6-455-465. – EDN: SQQGUT.

1. INTRODUCTION

The consumption of non-renewable energy (such as fossil, coal) and environmental problems are becoming increasingly serious, so, the demand for clean and sustainable energy such as hydrogen and solar energy has been increasing [1, 2]. Especially, hydrogen as a kind of clean renewable energy has received much attention because of its high energy (142,351 kJ/kg), no pollution and low cost [3, 4]. Water splitting, a promising method for hydrogen production [5], requires precious metal-based materials (like Pt, Pd, etc.) as catalysts to achieve robust catalytic performance. However, the scarcity and high cost of Pt-based and other precious metals-based catalysts have seriously hindered its widespread applications [2, 6]. Therefore, it is imperative to design and manufacture hydrogen evolution reaction (HER) catalysts with high cost-effective, resource-rich and high-performance advantages [7].

Among various candidates, metal nanodot-nitrogen-carbon (M–N–C) catalysts have been proved to be efficient catalysis due to their special coordination environment, which can adjust the electronic structure [6, 8–10]. Nanodot, a zero-dimensional material, has high specific surface area and higher catalyst utilization efficiency, which makes M–N–C catalyst have higher catalytic activity [11–13]. Carbon skeleton as the carrier of metal nanodots not only can effectively avoid agglomeration of nanodots, but as

a bridge between the nanodots also can effectively improve their electron transport performance [4, 14]. In addition, metal nitride (MN_x) and nitrogen-doped carbon (NC) can be produced by doping N element, which can improve the conductivity of the catalyst and increase the number of active sites [15–17]. For example, He and his colleagues prepared Ni–S–W–C electrode by pulse electrodeposition for hydrogen evolution reaction in alkaline electrolyte with an over-potential of 262 mV at a current density of 10 mA cm^{-2} [4]. Lin's team successfully prepared a dual-function electrode by encapsulating ultrafine FeNi alloy nanoparticles in N-doped layered carbon nanosheet for high-efficiency Zn-air batteries, which could be repeatedly charged and discharged for 1100 h at 5 mA cm^{-2} and for 600 h at 10 mA cm^{-2} [8]. Tian et al. recently large-scale prepared an economical, highly durable, and efficient catalyst (Pt_3Co alloy nanoparticles supported on carbon) for high-performance oxygen reduction reaction by the NaCl-template-assisted freeze drying approach as a simple and scalable method [18].

Based on the full consideration of the potential of M–N–C composites as an efficient catalyst, the W nanodot and nitrogen co-decorated carbon skeleton (W@NC) consisting of uniform tungsten nanodots (1.2 ± 0.6 nm) and interconnected N-doped carbon skeleton, was prepared for hydrogen evolution reaction. Specifically, the use of NaCl is the key to our strategy owing to that NaCl can not only act as a template to limit the growth of nanodots, but also participates in the pyrolysis reaction to improve the purity of phase. When used as HER catalyst, the W@NC electrode exhibited excellent HER performance in alkaline media with an over-potential of 228 mV at current density of 10 mA cm^{-2}.

2. EXPERIMENTAL SECTION

2.1. Preparation of W@NC Catalysts

W nanodots embedded N-doped carbon (W@NC) was prepared as follows. 150 mg $(NH_4)_6H_2W_{12}O_{40}$, 220 mg $C_{10}H_{16}N_2Na_2O_8Zn$, 20 mg $C_6H_{12}O_6$ and 1 g NaCl (cube crystals template owns the advantages of low cost, environmental friendliness, and ease of removal) were dissolved into 25 mL deionized (DI) water, and dry under –273°C. The as prepared precursor was annealed at 750°C for 2 h under Ar. The product was washed by DI water to remove NaCl and then dried at 60°C, defined as W@NC. For preparation of W@NC materials with lower and higher tungsten concentrations, 75 mg and 225 mg of $(NH_4)_6H_2W_{12}O_{40}$ were instead added into the precursor solution above, and the resulting samples were designated as W@NC-L and W@NC-H, respectively.

To explore the role of templates, tungsten@N-doped carbon composite was prepared without the addition of NaCl templates using the similar procedure.

2.2. Material Characterization

The field-emission scanning electron microscopy (FESEM; Zeiss SUPRA55) and transmission electron microscopy (TEM; JEOL, JEM-2200FS, 200kV) with energy dispersive X-ray spectroscopic (EDX) were used to observe the morphologies and structures of the catalyst. The catalysts were identified by X-ray diffraction (XRD) patterns (using a Rigaku Smartlab(3) D8 Advance X-ray diffractometer with Cu Kα radiation, λ = 1.5418 Å). The elemental chemical and surface electronic states of the samples were characterized by X-ray photoelectron spectroscopy (XPS, PHI5000 VersaProbe III with an Al Kα X-ray source). Raman spectra were collected by an HR800 UV micro-Raman spectrometer.

2.3. HER characterizations

All the HER measurements were performed on the CHI 660E electrochemical workstation (CH Instruments, Inc., Shanghai, China). 5 mg W@NC and 40 μL Nafion solution (5 wt%) were dispersed 960 mL ethanol and coated on Ni foam (1 cm × 1 cm) for vacuum drying overnight as working electrode. And the Hg/HgO electrode was used as reference electrode, graphite rod was used as the counter electrodes for a three electrode cell with 1 M KOH as electrolyte. And all potentials were calibrated to the RHE using the following equation: $E_{RHE} = E_{Hg/HgO} + 0.098 + 0.0591$ pH, (pH = 13.7 in 1 M KOH). The linear sweep voltammetry (LSV) curves without the iR-corrected were recorded at 2 mV s^{-1}. Cyclic voltammetry curve (CV) with different scanning rates (2 – 10 mV s^{-1}) were performed at the region (–0.043 ~ 0.057 V vs. RHE) avoiding Faradaic currents. Electrochemical impedance spectra (EIS) at an AC voltage (5 mV) were performed from 100 kHz to 10 mHz. The durability of hydrogen evolution reaction was evaluated by chronoamperometry.

3. RESULTS AND DISCUSSION

Fig. 1 illustrates the synthesis process of W@NC. First, the four components $(NH_4)_6H_2W_{12}O_{40}$, $C_{10}H_{16}N_2Na_2O_8Zn$, $C_6H_{12}O_6$ and NaCl were completely dissolved in DI water. The solution was freeze-dried to create precursor with a stable 3D assembly. Subsequently, the precursor was annealed in Ar to produce the W@NC/NaCl. During the annealing process, the in situ reaction took place between $(NH_4)_6H_2W_{12}O_{40}$ and $C_{10}H_{16}N_2Na_2O_8Zn$ on the surface of NaCl template, forming uniform W nanodots embedded in N-doped carbon matrix. Finally, the NaCl template was removed with DI water to obtain W@NC. The morphology and physicochemical properties of the sample may be influenced by different W/C ratio, which can affect the catalytic performance. Therefore, in order to obtain the optimal HER catalyst, a similar synthe-

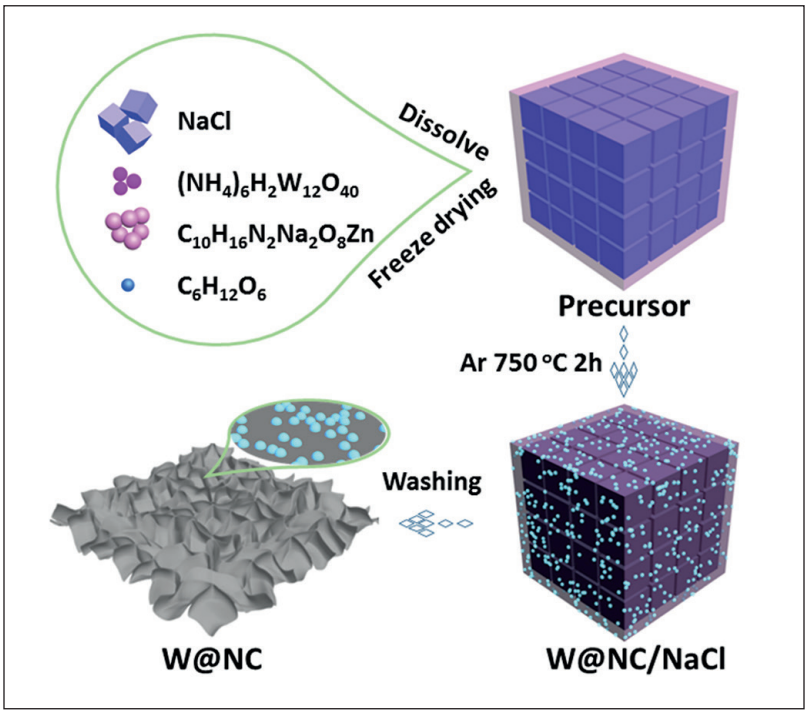

Fig. 1. **Schematic illustration of the preparation process for the W@NC**

sis process was used to prepare samples with different amounts of $(NH_4)_6H_2W_{12}O_{40}$ (75, 150 and 225 mg), named W@NC-L, W@NC and W@NC-H, respectively.

The effect of $(NH_4)_6H_2W_{12}O_{40}$ usage on the morphology and phase was studied in Fig. 2. As expected, the morphology of W@NC-L, W@NC, and W@NC-H are based on carbon skeletons. With the increase of tungsten content, nanodots or nanoparticles could be observed on the carbon skeleton, and the diffraction peak intensity of tungsten nitride (WN) increased gradually. It was clear that the morphology of W@NC-L was identical with carbon skeleton (Fig. 2a), and the XRD pattern (Fig. 2b) of the W@NC-L distinctly exhibited a significant diffraction peak at around 26.2°, which was assigned to the C

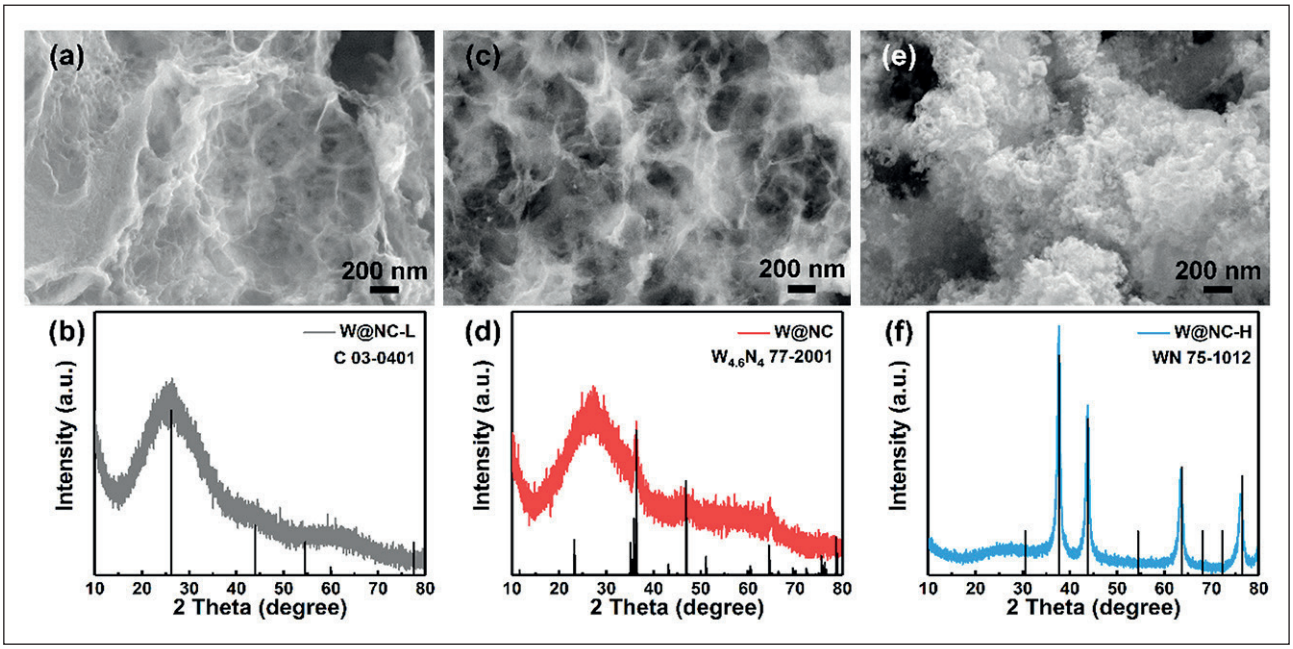

Fig. 2. **SEM images and XRD patterns of (a and b) W@NC-L, (c and d) W@NC and (e and f) W@NC-H**

(JCPDS card No. 03-0401). It is noteworthy that a few nanodots were observed on the carbon skeleton in W@NC (Fig. 2c), and obvious nanoparticles were observed on the carbon skeleton in W@NC-H (Fig. 2e), indicating that nanodots inevitably agglomerated into nanoparticles with W dosage greater than 150 mg. The diffraction peaks of W@NC (Fig. 2d) at 36.3, 46.8 and 64.4° corresponded to $W_{4.6}N_4$ (JCPDS card No. 77-2001). And the diffraction peaks of W@NC-H (Fig. 2f) at 37.6, 43.8, 63.6 and 76.4° corresponded to WN (JCPDS card No. 75-1012). The characteristic peaks for W@NC provided direct evidence for the existence of W and C in the hybrid.

The graphite degree of carbon in the hybrid was further studied by Raman spectroscopy (Fig. 3a). The peaks around 1353 and 1583 cm^{-1} correspond to the D (the disordered sp^2-hybridized carbon) and G (the result of the highly ordered graphite) bands of the carbon, respectively [19, 20]. Compared with those of the W@NC-L, the G band of the W@NC shifted up to 1587cm^{-1}, indicating the successful doping of the N atoms [17]. Meanwhile, the I_D/I_G of W@NC (1.098) was the same as that of W@NC-L (1.098), which was slightly smaller than W@NC-H (1.151), indicating the almost similar degree of graphitization. However, the vibration peaks of W@NC-H (Fig. 3b) at 695 and 800 cm^{-1} corresponded to the Raman peaks of WN, confirming the successful preparation of the WN [17, 21].

In addition, it is notable that NaCl plays a key role in the successful preparation of W@NC. For comparison, the tungsten@N-doped carbon composites without NaCl present obvious nanoparticle structure (Fig. 4a and b), and its XRD diffraction peaks (Fig. 4c) are inconsistent with that of W@NC, which is reasonable to infer that NaCl can not only limit the growth of nanodots to regulate the morphology of materials, but also participates in the pyrolysis reaction to improve the purity of phase.

The morphology and structure of the W@NC hybrid were further investigated by TEM. The TEM image (Fig. 5a and b) clearly reveals that the tungsten nanodots were uniformly distributed on interconnected carbon skeletons. The size distribution of W nanodots (Fig. 5c) conforms to a normal probability distribution, and the size of the nanodots was around 1.2 ± 0.6 nm. The black dot in high resolution TEM (HRTEM, Fig. 5d) and the dispersion ring in selected area electron diffraction (SAED, Fig. 5e) results suggested that W nanodots did not aggregate into nanoparticles [10]. Besides, the elemental mapping of C, W and O in W@NC hybrid (Fig. 5f) showed

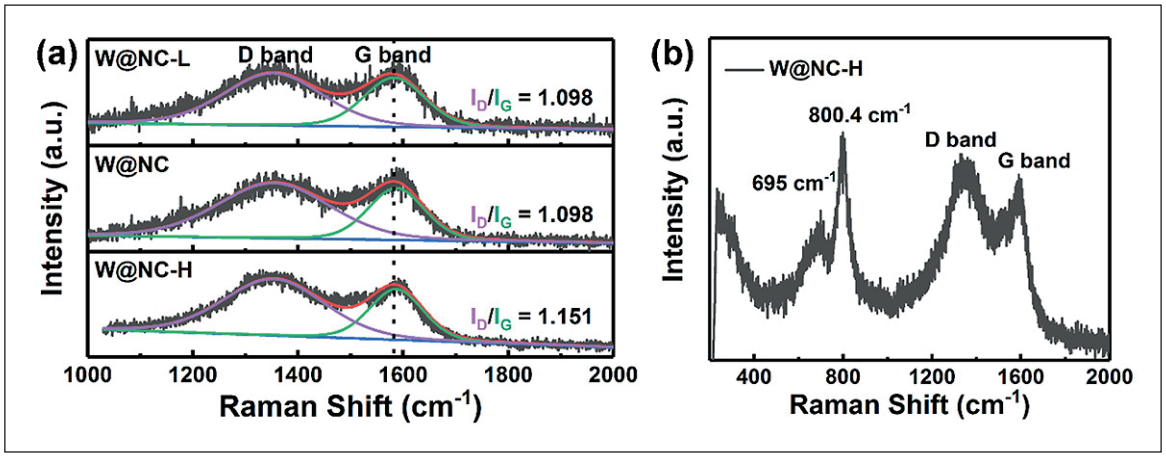

Fig. 3. **Raman spectra of W@NC-L, W@NC and W@NC-H**

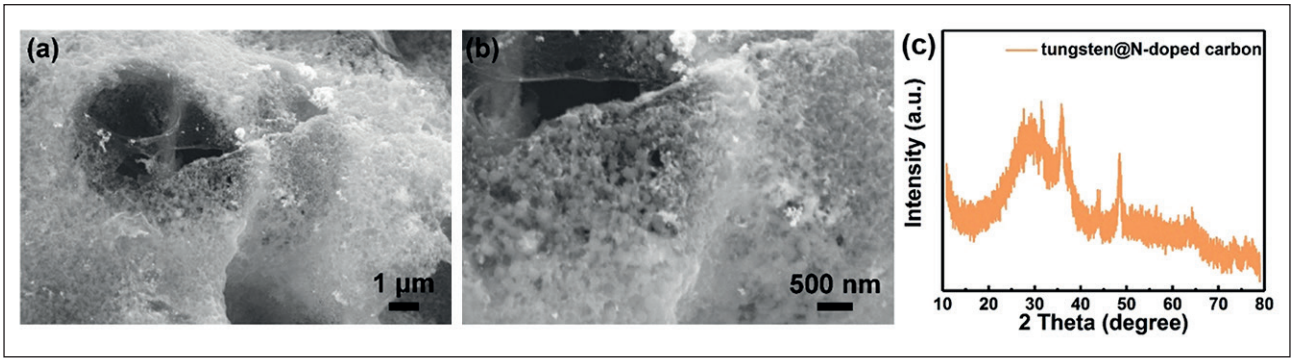

Fig. 4. **(a, b) SEM images and (c) XRD pattern of tungsten@N-doped carbon composite without NaCl**

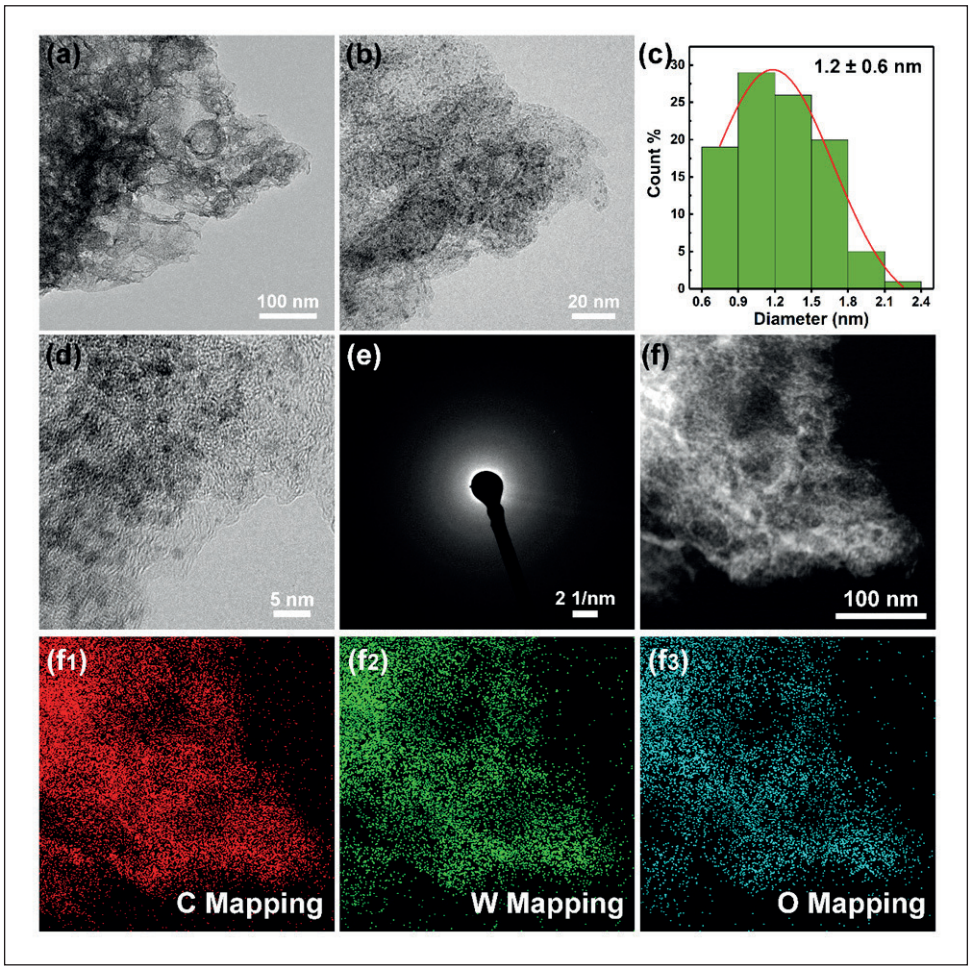

Fig. 5. **(a and b) TEM images at different magnifications, (c) Histogram of particle size distribution, (d) HRTEM image, (e) SAED pattern and (f) Dark-field FE-TEM image with EDS mapping images of W@NC**

that all element were evenly distributed in the material. Noting that the absence of an N signal may be due to nitrogen levels below the instrument's detection limit.

The surface composition and chemical states of W@NC hybrids were also determined by X-ray photoelectron spectroscopy (XPS). The survey XPS spectrum in Fig. 6 reveals that the surface of W@NC consisted of C (72.9%), W (3.2%), N (8.8%) and O (15%) elements, which indicates that N was doped in the carbon skeleton. The high-resolution C 1s spectrum in Fig. 7a can be split into four peaks. The peaks centered at 284.8, 285.9, 286.8 and 288.2 eV corresponds to the C = C, the C–N, C–O and C = O bonds, respectively [22, 23]. The high resolution spectrum of W 4f can be deconvoluted into two doublets (Fig. 7b). Two peaks at 33.3 and 35.6 eV were ascribed to W^{4+}, and the other two peaks at high band energy (35.8 and 38.0 eV) belonged to W^{6+}, which is the predominate component of W in W@NC hybrid [24]. The N 1s spectrum (Fig. 7c) shows three peaks at 398.5 eV, 400.4 eV and 402.0 eV, which were indexed to pyridinic N, pyrrolic N and graphitic N, respectively [6, 22]. Additionally,

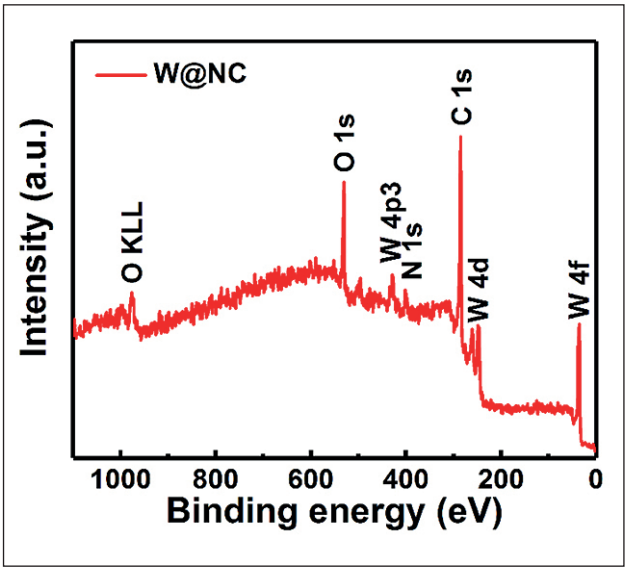

Fig. 6. **XPS survey of W@NC**

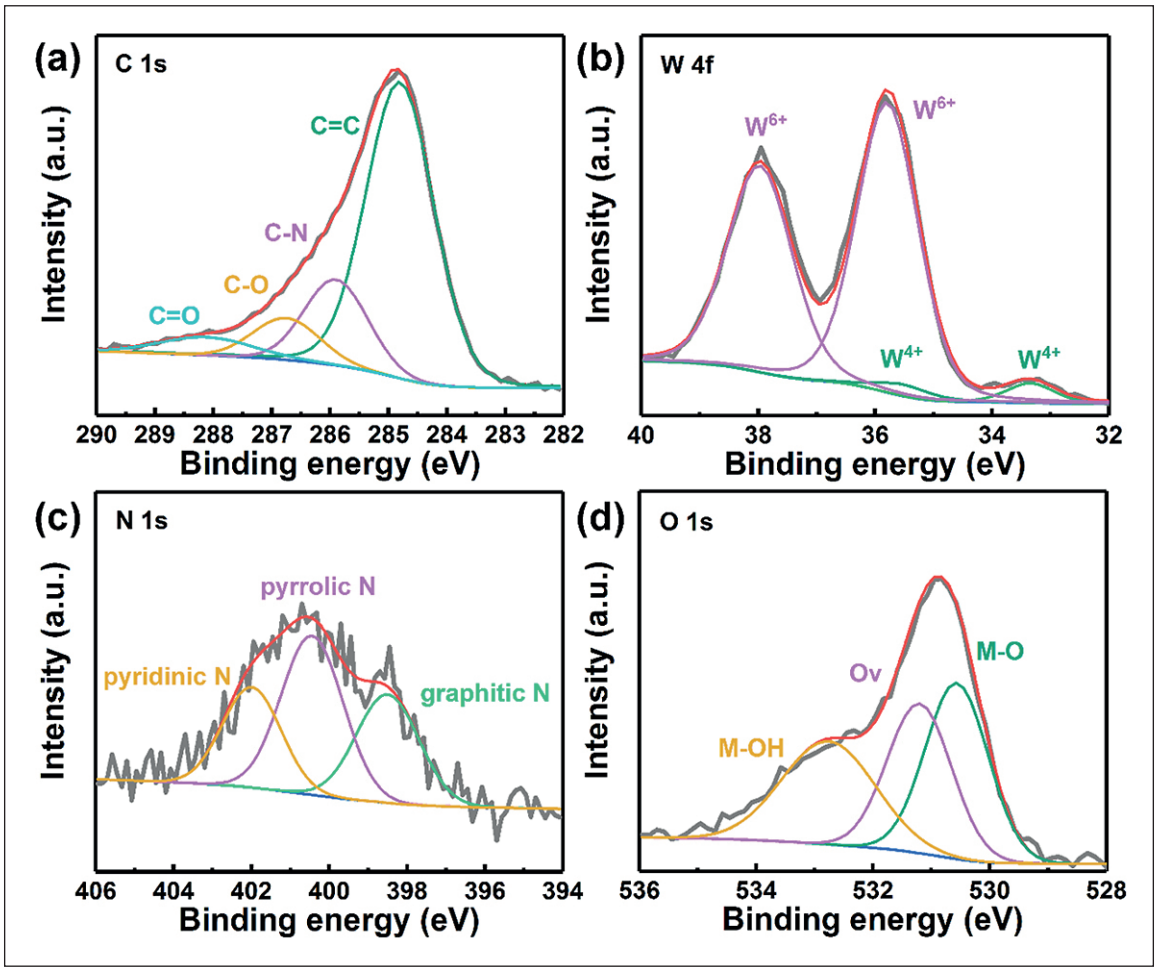

Fig. 7. **The XPS spectra of (a) C 1s, (b)W 4f, (c)N 1s and (d) O 1s in W@NC**

the XPS spectra of O 1s (Fig. 7d) confirms the existence of oxygen vacancy (O_v, 531.2 eV), lattice oxygen atoms of metal-oxygen (M-O, 530.5 eV) and surface-adsorbed hydroxyl group (M-OH, 532.8 eV) in the sample [25, 26].

The hydrogen evolution activities of all catalysts were evaluated by linear scanning voltammetry (LSV) in Ar-saturated 1 M KOH. Fig. 8a shows the polarization curves without iR-compensation at a scan rate of 2 mV s^{-1}. The W@NC exhibited optimal catalytic HER performance with 228 mV over-potential at a current density of 10 mA cm^{-2}, which is comparable to that of recently reported non-noble metal catalysts (Tab. 1). The LSV curve of W@NC-H almost coincides with that of W@NC, and the performance was better than that of W@NC-L, indicating that the hydrogen evolution performance reaches saturation when the dosage of W was 150 mg. Tafel slope in Fig. 8b was obtained by linear fitting of polarization curve. Noting that the Tafel slope of W@NC (165.8 mV dec^{-1}) was similar to W@NC-H (165.4 mV dec^{-1}), which was lower than that of W@NC-L (210.4 mV dec^{-1}). The lower Tafel slope value indicated that the reaction dynamics processes of W@NC and W@NC-H were relatively faster and thus HER activity was higher. Fig. 8c shows the Nyquist plots of catalysts at −0.19 V vs. RHE. The charge transfer resistance (R_{ct}) of the material decreased with the increase of W content, indicating that HER electron dynamics accelerates with the increase of W content [27, 28]. However, the R_{ct} of W@NC-H (7.97 ohm) was similar with that of W@NC (8.35 ohm), indicating that when the W content is greater than 150 mg, its influence on R_{ct} decreases.

In order to further explore the effect of W content on the electrochemical active surface area (ECSA), the cyclic voltammetry of the material (Fig. 9) was measured in the region without Faradaic currents at scan rates varying from 2 to 10 mV s^{-1} to calculate the double layer capacitance (C_{dl}), which is proportional to ECSA [7, 29-32]. As shown in Fig. 8d, the C_{dl} values were ranked as follows: W@NC-L (236.2 mF cm^{-2}) > W@NC (219.9 mF cm^{-2}) >> W@NC-H (91.4 mF cm^{-2}), indicating that high loading will reduce the active specific surface area. Based on the above analysis, the optimal HER activity of W@NC can be ascribed to the optimal synergistic catalytic effect between the active W nanodots

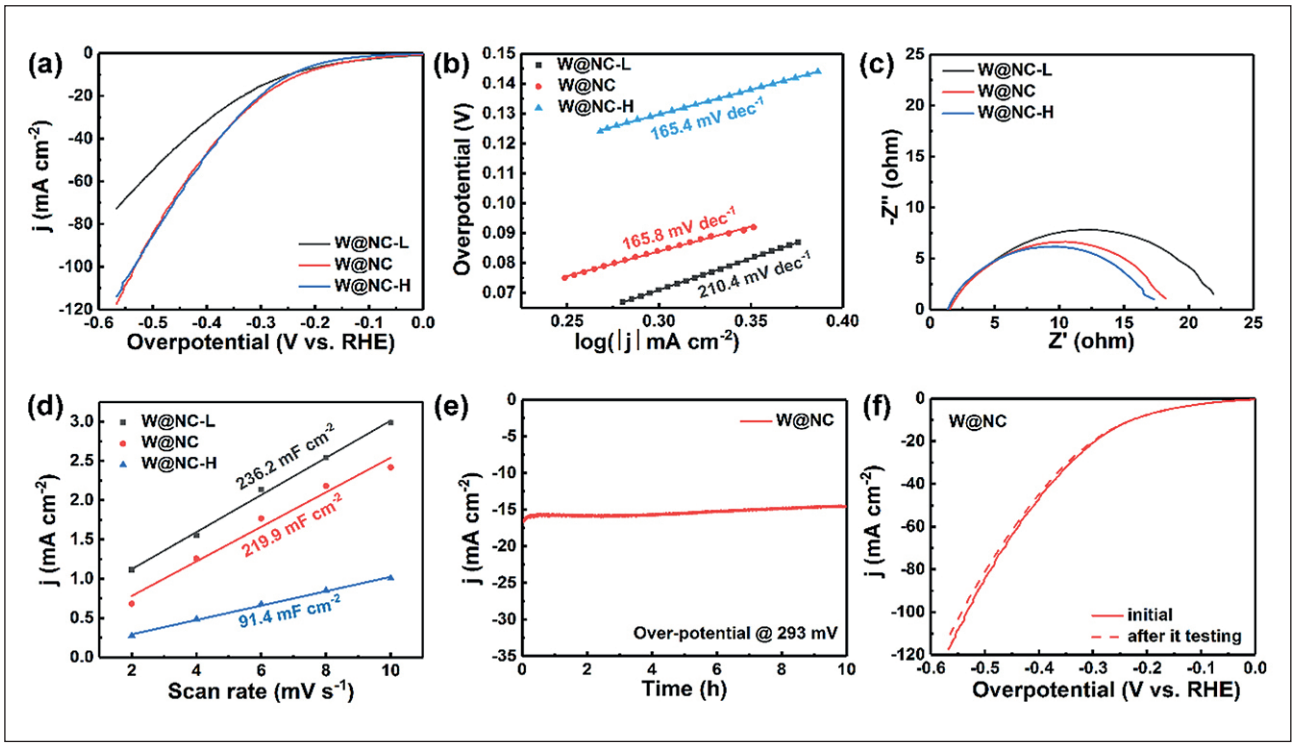

Fig. 8. **(a) Polarization curves without iR correction, (b) Tafel plots, (c) EIS Nyquist plots and (d) C_{dl} for W@NC-L, W@NC and W@NC-H. (e) Time dependence of current density under static over-potential of 293 mV for W@NC. (f) Polarization curves without iR correction of the W@NC before and after i-t tasting**

Table 1
Summary of HER properties on our W@NC catalyst and the reported catalysts

Catalysts	Over-potential at 10 mA cm^{-2} (mV)	Tafel slope (mV dec^{-1})	Electrolyte	References
W@NC	228	165.8	1 M KOH	This work
Ni-S-W-C	262	105	30% KOH	[4]
Mo_2C	262	114	1 M KOH	[7]
WN	571	164.0	1 M KOH	[22]
WC_{1-X}	216	122.2	1 M KOH	[22]
Meso-$WO_{2.83}$	287	95	1 M KOH	[25]
O_v-WO_x@NC	434@20	125	1 M KOH	[26]
WN NA/CC	285	92	1 M KOH	[33]
b	332	136	1 M KOH	[34]
WC	227	142.4	1 M KOH	[35]
WN	313@20	118	1 M KOH	[36]
W/WO_2 NA@CP	297	74.5	1 M KOH	[37]
WNx-NRC	255	115	0.5 M H_2SO_4	[38]
WS_3	704	109	0.5 M H_2SO_4	[39]
C-WP	216	59	0.5 M H_2SO_4	[40]
WS_x@OMC	213	74	0.5 M H_2SO_4	[41]

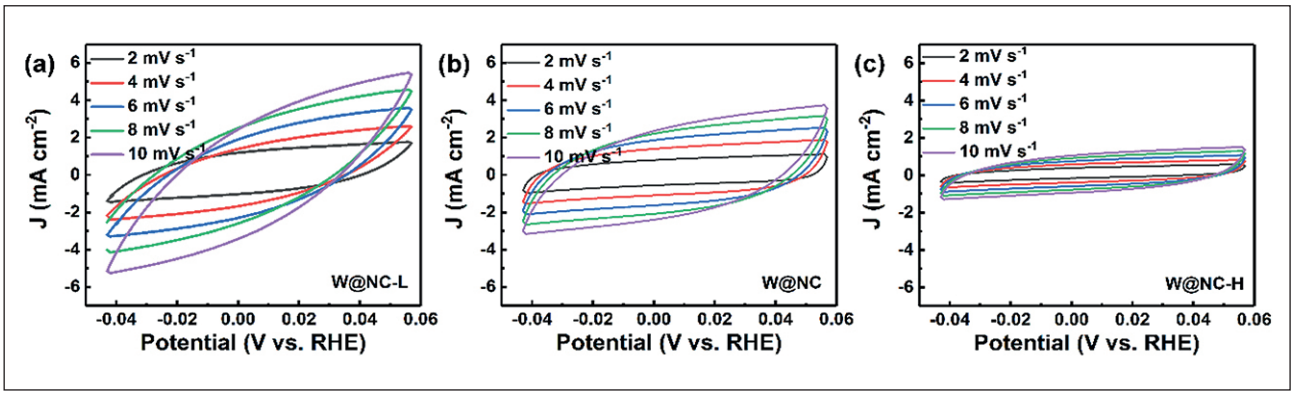

Fig. 9. **CV curves of (a) W@NC-L, (b) W@NC and (c) W@NC-H with different rates from 2 to 10 mV s^{-1}**

and the conductive carbon skeleton. The long-term stability of W@NC at a constant over-potential of 293 mV was evaluated by chronoamperometry. As shown in Fig. 8e, the current density almost remained unchanged, and the negligible degradation could be ignored after the continuous test over 10 h. And the polarization curve of W@NC catalyst after 10 h stability test showed negligible decay (Fig. 8f).

Based on the above results of electrochemical study, the increased catalytic activity of W@NC can be attributed to the following reasons: 1) The unique structure can increase the contact area between catalyst and electrolyte, which is more conducive to mass charge transfer. 2) N-doped conductive C skeleton not only facilitates electron transfer, but also acts as a "spacer" to effectively prevent W nanodots from agglomeration. 3) An appropriate amount of W nanodots was uniformly anchored on the carbon matrix, more effectively exposing the active sites.

4. CONCLUSIONS

In this work, the W nanodots and nitrogen co-decorated carbon skeleton (W@NC) was prepared for alkaline hydrogen evolution reaction. The interconnected carbon skeleton not only prevents the agglomeration of W nanodots, but also provides a good conductive substrate. By optimizing the loading capacity of W nanodots, W@NC has the best performance (a lower over-potential of 228 mV at 10 mA cm^{-2} and long-term operation over 10 h) when W dosage is 2 mM. The excellent electrochemical performance of the W@NC hybrid may be ascribed to the synergistic effect between uniformly dispersed W nanodots and conductive N-doped carbon skeleton.

REFERENCES

1. Hu Y., Yu B., Li W.X., Ramadoss M., Chen Y.F. W_2C nanodot-decorated CNT networks as a highly efficient and stable electrocatalyst for hydrogen evolution in acidic and alkaline media. Nanoscale. 2019: 11(11): 4876-4884. https://doi.org/10.1039/c8nr10281c

2. Shi M.Q., Jiang Z.Z., Mei B.B., Li Y.Y., Sun F.F., Yu H.S., Xu Y.H. Tuning the hydrogen evolution performance of 2D tungsten disulfide by interfacial engineering. *J. Mater. Chem. A.* 2021: 9(11): 7059-7067. https://doi.org/10.1039/d0ta10673a

3. Shan A.X., Teng X.A., Zhang Y.,Zhang P.F., Xu Y.Y., Liu C.R., Li H., Ye H.Y., Wang R.M. Interfacial electronic structure modulation of Pt-MoS_2 heterostructure for enhancing electrocatalytic hydrogen evolution reaction. *Nano Energy.* 2022: 94: 106913. https://doi.org/10.1016/j.nanoen.2021.106913

4. Wu Y.H., He H.W. A novel Ni-S-W-C electrode for hydrogen evolution reaction in alkaline electrolyte. *Mater. Lett.* 2019: 209: 532-534. https://doi.org/10.1016/j.matlet.2017.08.086

5. Lin Z.P., Xiao B.B., Wang Z.P., Tao W.Y., Shen S.J., Huang L.A., Zhang J.T., Meng F.Q., Zhang Q.H., Gu L., Zhong W.W. Planar-coordination $PdSe_2$ nanosheets as highly active electrocatalyst for hydrogen evolution reaction. *Adv. Funct. Mater.* 2021: 31(32): 2102321. https://doi.org/10.1002/adfm.202102321

6. Li C.F., Zhao J.W., Xie L.J., Wu J.Q., Li G.R. Water adsorption and dissociation promoted by Co*-/N-C*-biactive sites of metallic Co/N-doped carbon hybrids for efficient hydrogen evolution. *Appl. Catal. B-Environ.* 2021: 282: 119463. https://doi.org/10.1016/j.apcatb.2020.119463

7. Yang C.F., Zhao R., Xiang H., Wu J., Zhong W.D., Li W.L., Zhang Q., Yang N.J., Li X.K. Ni-activated transition metal carbides for efficient hydrogen evolution in acidic and alkaline solutions. *Adv. Energy Mater.* 2020: 10(37): 2002260. https://doi.org/10.1002/aenm.202002260

8. Li X.F., Liu Y.J., Chen H.B., Yang M., Yang D.G., Li H.M., Lin Z.Q. Rechargeable Zn-air batteries with outstanding cycling stability enabled by ultrafine FeNi nanoparticles-encapsulated N-doped carbon nanosheets as a bifunctional electrocatalyst. *Nano Lett.* 2021: 21(7): 3098-3105. https://doi.org/10.1021/acs.nanolett.1c00279

9. Zhang Z.H., Yang X.N., Liu K.H., Wang R.M. Epitaxy of 2D Materials toward Single Crystals. *Adv. Sci.* 2022: 9(8): 2105201. https://doi.org/10.1002/advs.202105201

10. Bisen O.Y., Yadav A.K., Nanda K.K. Self-organizedsingle-atom tungsten supported on the N-doped carbon matrix for durable oxygen reduction. *ACS Appl. Mater. Inter.* 2020: 12(39): 43586-43595. https://doi.org/10.1021/acsami.0c10234

11. Qu Y.T., Wang L.G., Li Z.J., Li P., Zhang Q.H., Lin Y., Zhou F.Y., Wang H.J., Yang Z.K., Hu Y.D., Zhu M.Z., Zhao X.Y., Han X., Wang C.M., Xu Q., Gu L., Luo J., Zheng L.R., Wu Y.E. Ambient synthesis of single-atom catalysts from bulk metal via trapping of atoms by surface dangling bonds. *Adv. Mater.* 2019: 31(44): 1904496-1902503. https://doi.org/10.1002/adma.201904496

12. Zhang L.L., Liu D.B., Muhammad Z., Wan F., Xie W., Wang Y.J., Song L., Niu Z.Q., Chen J. Single nickel atoms on nitrogen-doped graphene enabling enhanced kinetics of lithium-sulfur batteries. *Adv. Mater.* 2019: 31(40): 1903955. https://doi.org/10.1002/adma.201903955

13. Zhang E.H., Wang T., Yu K., Liu J., Chen W.X., Li A., Rong H.P., Lin R., Ji S.F., Zheng X.S., Wang Y., Zheng L.R., Chen C., Wang D.S., Zhang J.T., Li Y.D. Bismuth single atoms resulting from transformation of metal-organic frameworks and their use as electrocatalysts for CO_2 reduction. *J. Am. Chem. Soc.* 2019: 141(42): 16569-16573. https://doi.org/10.1021/jacs.9b08259

14. Wei R.C., Gu Y., Zou L.L., Xi B.J., Zhao Y.X., Ma Y.N., Qian Y.T., Xiong S.L., Xu Q. Nanoribbon superstructures of graphene nanocages for efficient electrocatalytic hydrogen evolution. *Nano Lett.* 2020: 20(10): 7342-7349. https://doi.org/10.1021/acs.nanolett.0c02766

15. Zhao L., Zhang Y., Huang L.B., Liu X.Z., Zhang Q.H., He C., Wu Z.Y., Zhang L.J., Wu J., Yang W., Gu L., Hu J.S., Wan L.J. Cascade anchoring strategy for general mass production of high-loading single-atomic metal-nitrogen catalysts. *Nat. Commun.* 2019: 10: 1278. https://doi.org/10.1038/s41467-019-09290-y

16. Liu Z.Z., Zhang X.M., Song H., Yang Y.X., Zheng Y., Gao B., Fu J.J., Chu P.K., Huo K.F. Electronic modulation between tungsten nitride and cobalt dopants for enhanced hydrogen evolution reaction at a wide range of pH. *ChemCatChem.* 2020: 12(11): 2962-2966. https://doi.org/10.1002/cctc.202000391

17. Zhang J., Chen J.W., Luo Y., Chen Y.H., Wei X.Y., Wang G., Wang R.L. Sandwich-like electrode with tungsten nitride nanosheets decorated with carbon dots as efficient electrocatalyst for oxygen reduction. *Appl. Surf. Sci.* 2019: 466: 911-919. https://doi.org/10.1016/j.apsusc.2018.10.116

18. Han X.F., Batool N., Wang W.T., Teng H.T., Zhang L., Yang R., Tian J.H. Templated-assisted synthesis of structurally ordered intermetallic Pt_3Co with ultralow loading supported on 3D porous carbon for oxygen reduction reaction. *ACS Appl. Mater. Inter.* 2021: 13(31): 37133-37141. https://doi.org/10.1021/acsami.1c08839

19. Wu Q., Liang J., Yi J.D., Shi P.C., Huang Y.B., Cao R. Porous nitrogen/halogen dual-doped nanocarbons derived from imidazolium functionalized cationic metal-organic frameworks for highly efficient oxygen reduction reaction. *Sci. China Mater.* 2018: 62(5): 671-680. https://doi.org/10.1007/s40843-018-9364-5

20. Teng X.A., Shan A.X., Zhu Y.C., Wang R.M., Lau W.M. Promoting methanol-oxidation-reaction by loading PtNi nano-catalysts on natural graphitic-nano-carbon. *Electrochim. Acta.* 2020: 353: 136542. https://doi.org/10.1016/j.electacta.2020.136542

21. He D.Q., Xiang J.L., Zha C.Y., Wu R., Deng J., Zhao Y.W., Xie H.G., Liu Y., Wang P.C., Wang W., Yin Y., Qin T.S., Zhu C., Rao Z.H., Wang L., Huang W. The efficient redox electron transfer and powered polysulfide confinement of carbon doped tungsten nitride with multi-active sites towards high-performance lithium-polysulfide batteries. *Appl. Surf. Sci.* 2020: 525: 146625. https://doi.org/10.1016/j.apsusc.2020.146625

22. Tong R., Qu Y.J., Zhu Q., Wang X.N., Lu Y.H., Wang S.P., Pan H. Combined experimental and theoretical assessment of WX_y (X = C, N, S, P) for hydrogen evolution reaction. *ACS Appl. Energy Mater.* 2020: 3(1): 1082-1088. https://doi.org/10.1021/acsaem.9b02114

23. Yan H.J., Meng M.C., Wang L., Wu A.P., Tian C.G., Zhao L., Fu H.G. Small-sized tungsten nitride anchoring into a 3D CNT-rGO framework as a superior bifunctional catalyst for the methanol oxidation and oxygen reduction reactions. *Nano Res.* 2015: 9(2): 329-343. https://doi.org/10.1007/s12274-015-0912-x

24. Ling Y., Kazim F., Ma S.X., Zhang Q., Qu K.G., Wang Y.G., Xiao S.L., Cai W.W., Yang Z.H. Strain induced rich planar defects in heterogeneous WS_2/WO_2 enable efficient nitrogen fixation at low overpotential. *J. Mater. Chem. A.* 2020: 8(26): 12996-13003. https://doi.org/10.1039/c9ta13812a

25. Cheng H.F., Klapproth M., Sagaltchik A., Li S., Thomas A. Ordered mesoporous $WO_{2.83}$: Selective Reduction Synthesis, Exceptional localized surface plasmon resonance and enhanced hydrogen evolution reaction activity. *J. Mater. Chem. A.* 2018: 6(5): 2249-2256. https://doi.org/10.1039/c7ta09579a

26. Lv C.C., Yan G.Y., Wang X.B., Gao L.J., Xu S.C., San X.Y., Wang S.F., Li Y.G., Huang Z.P. Ni loaded on N-doped carbon encapsulated tungsten oxide nanowires as an alkaline-stable electrocatalyst for water reduction. *Sustain. Energy. Fuels.* 2020: 4(2): 788-796. https://doi.org/10.1039/c9se00616h

27. Zhang H.F., Pan Q., Sun Z.P., Cheng C.W. Three-dimensional macroporous W_2C inverse opal arrays for the efficient hydrogen evolution reaction. *Nanoscale.* 2019: 11(24): 11505-11512. https://doi.org/10.1039/c9nr03548f

28. Feng Q., Xiong Y.Y.H., Xie L.J., Zhang Z., Lu X.E., Wang Y.J., Yuan X.Z., Fan J.T., Li H., Wang H.J. Tungsten carbide encapsulated in grape-like N-doped carbon nanospheres: one-step facile synthesis for low-cost and highly active electrocatalysts in proton exchange membrane water electrolyzers. *ACS Appl. Mater. Inter.* 2019: 11(28): 25123-25132. https://doi.org/10.1021/acsami.9b04725

29. Lin H.L., Liu N., Shi Z.P., Guo Y.L., Tang Y., Gao Q.S. Cobalt-doping in molybdenum-carbide nanowires toward efficient electrocatalytic hydrogen evolution. *Adv. Funct. Mater.* 2016: 26(31): 5590-5598. https://doi.org/10.1002/adfm.201600915

30. Li W.R., Zhao H.F., Li H., Wang R.M. Fe doped NiS nanosheet arrays grown on carbon fiber paper for a highly efficient electrocatalytic oxygen evolution reaction. Nanoscale Adv. 2022: 4(4): 1220-1226. https://doi.org/10.1039/d2na00004k

31. Lv Y.P., Duan S.B., Zhu Y.C., Yin P., Wang R.M. Enhanced OER performances of Au@ $NiCo_2S_4$ core-shell heterostructure. *Nanomaterials.* 2020: 10(4): 611. https://doi.org/10.3390/nano10040611

32. Lv Y.P., Duan S.B., Zhu Y.C., Guo H.Z., Wang R.M. Interface control and catalytic performances of Au-NiS_x heterostructures. *Chem. Eng. J.* 2020: 382: 122794. https://doi.org/10.1016/j.cej.2019.122794

33. Shi J.L., Pu Z.H., Liu Q., Asiri A. M., Hu J.M., Sun X.P. Tungsten nitride nanorods array grown on carbon cloth as an efficient hydrogen evolution cathode at all pH values. *Electrochim. Acta.* 2015: 154: 345-351. https://doi.org/10.1016/j.electacta.2014.12.096

34. Jin H.Y., Zhang H., Chen J.Y., Mao S.J., Jiang Z., Wang Y., A general synthetic approach for hexagonal phase tungsten nitride composites and their application in the hydrogen evolution reaction. *J. Mater. Chem. A.* 2018: 6(23): 10967-10975. https://doi.org/10.1039/c8ta02595a

35. Abbas S.C., Wu J., Huang Y., Babu D.D., Anandhababu G., Ghausi M.A., Wu M., Wang Y., Novel strongly coupled tungsten-carbon-nitrogen complex for efficient hydrogen evolution reaction. *Inter. J. Hydrog. Energ.* 2018: 43(1): 16-23. https://doi.org/10.1016/j.ijhydene.2017.11.065

36. Lv C.C., Wang X.B., Gao L.J., Wang A.J., Wang S.F., Wang R.N., Ning X.K., Li Y.G., Boukhvalov D.W., Huang Z.P., Zhang C. Triple functions of $Ni(OH)_2$ on the surface of WN nanowires remarkably promoting electrocatalytic activity in full water splitting. *ACS Catal.* 2020: 10(22): 13323-13333. https://doi.org/10.1021/acscatal.0c02891

37. Zhao Y.X., Lv C.C., Huang Q.L., Huang Z.P., Zhang C. Self-supported tungsten/tungsten dioxide nanowires array as an efficient electrocatalyst in hydrogen evolution reaction. *RSC Adv.* 2016: 6(92): 89815-89820. https://doi.org/10.1039/c6ra17194j

38. Zhu Y.P., Chen G., Zhong Y.J., Zhou W., Shao Z.P. Rationally designed hierarchically structured tungsten nitride and nitrogen-rich graphene-like carbon nanocomposite as efficient hydrogen evolution electrocatalyst. *Adv. Sci.* 2018: 5(2): 1700603. https://doi.org/10.1002/advs.201700603

39. Latiff N.M., Wang L., Mayorga-Martinez C.C., Sofer Z., Fisher A.C., Pumera M. Valence and oxide impurities in MoS_2 and WS_2 dramatically change their electrocatalytic activity towards proton reduction. *Nanoscale.* 2016: 37: 16752-16760. https://doi.org/10.1039/c6nr03086f

40. Zhang X.Y., Guo T., Liu T.Y., Lv K.Y., Wu Z.Z., Wang D.Z., Tungsten phosphide (WP) nanoparticles with tunable crystallinity, W vacancies, and electronic structures for hydrogen production. *Electrochim. Acta.* 2019: 323(10): 134798. https://doi.org/10.1016/j.electacta.2019.134798

41. Seo B., Jung G.Y., Kim J.H., Shin T.J., Jeong H.Y., Kwak S.K., Joo S.H. Preferential horizontal growth of tungsten sulfide on carbon and insight into active sulfur sites for the hydrogen evolution reaction. *Nanoscale.* 2018: 10(8): 3838-3848. https://doi.org/10.1039/c7nr08161h

INFORMATION ABOUT THE AUTHORS

Yange Wang – Ph. D, student, Beijing Advanced Innovation Center for Materials Genome Engineering, Beijing Key Laboratory for Magneto-Photoelectrical Composite and Interface Science, Center for Green Innovation, University of Science and Technology Beijing, Beijing, 100083, China, E-mail: wygnjzy@163.com

Yechen Wang – M.Sc., student, Beijing Advanced Innovation Center for Materials Genome Engineering, Beijing Key Laboratory for Magneto-Photoelectrical Composite and Interface Science, Center for Green Innovation, University of Science and Technology Beijing, Beijing, 100083, China, E-mail: s20190809@xs.ustb.edu.cn

Jing Bai – Ph. D, lecturer, Beijing Advanced Innovation Center for Materials Genome Engineering, Beijing Key Laboratory for Magneto-Photoelectrical Composite and Interface Science, Center for Green Innovation, University of Science and Technology Beijing, Beijing, 100083; Shunde Graduate School of University of Science and Technology Beijing, Foshan 528000, China, xingqingcaoyuan@163.com

Sibin Duan – Ph. D, associate professor, Beijing Advanced Innovation Center for Materials Genome Engineering, Beijing Key Laboratory for Magneto-Photoelectrical Composite and Interface Science, Center for Green Innovation, University of Science and Technology Beijing, Beijing, 100083, China, E-mail: sibinduan@ustb.edu.cn

Rongming Wang – Ph. D, professor, Beijing Advanced Innovation Center for Materials Genome Engineering, Beijing Key Laboratory for Magneto-Photoelectrical Composite and Interface Science, Center for Green Innovation, University of Science and Technology Beijing, Beijing, 100083, China, rmwang@ustb.edu.cn

Woon-Ming Lau – Ph. D, professor, Beijing Advanced Innovation Center for Materials Genome Engineering, Beijing Key Laboratory for Magneto-Photoelectrical Composite and Interface Science, Center for Green Innovation, University of Science and Technology Beijing, Beijing, 100083; Shunde Graduate School of University of Science and Technology Beijing, Foshan 528000, China, leolau@ustb.edu.cn

CONTRIBUTION OF THE AUTHORS

The authors contributed equally to this article.

The authors declare no conflicts of interests.

The article was submitted 20.10.2022; approved after reviewing 14.11.2022; accepted for publication 17.11.2022